SUPPLEMENTARY INFORMATION

Evidence for a group II intron-like catalytic triplex in the spliceosome

Sebastian M. Fica, Melissa A. Mefford, Joseph A. Piccirilli, and Jonathan P. Staley

SUPPLEMENTARY FIGURES

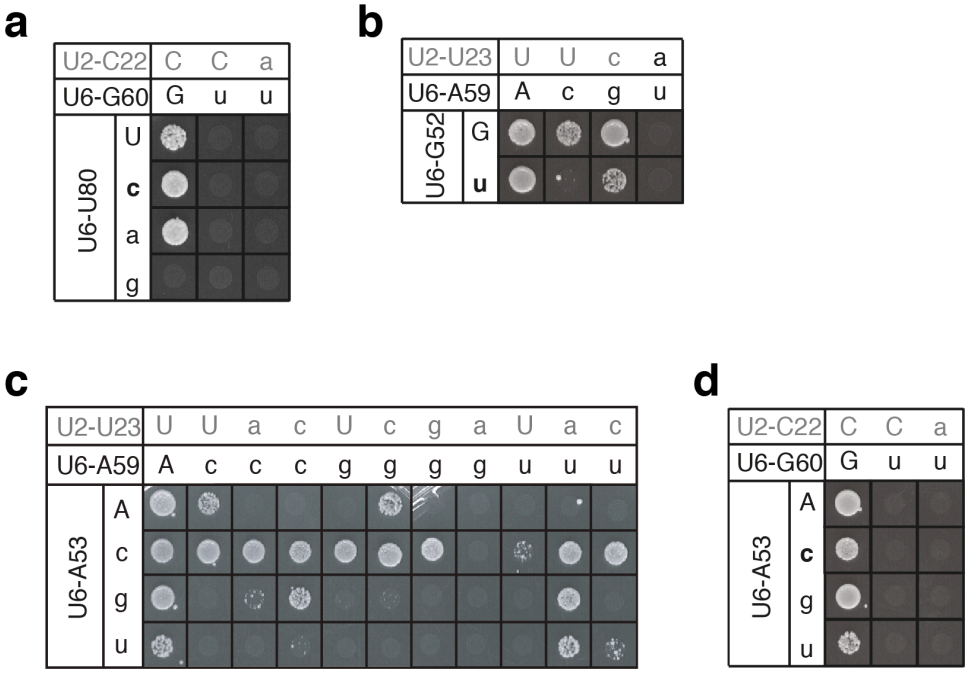

Supplementary Figure 1. Further evidence that mutations in predicted base triple partners only suppress AGC triad mutations in the same plane of the predicted triplex. (a-d), Spot assays showing growth on selective media of equivalent numbers of yeast cells containing combinations of alleles at U80 and G60 (**a**), G52 and A59 (**b**), A53 and A59 (**c**), or A53 and G60 (**d**). The allele combinations for the U2/U6 helix Ib base pair mutated in each case are indicated above each panel, and the allele of the predicted base triple partner is shown to the left of each panel. Note that at each triad position, at least one mutation shown here as not suppressed by an out-of-the-plane mutation in the predicted triplex is nevertheless suppressed by an in-the-plane mutation of the predicted triplex.

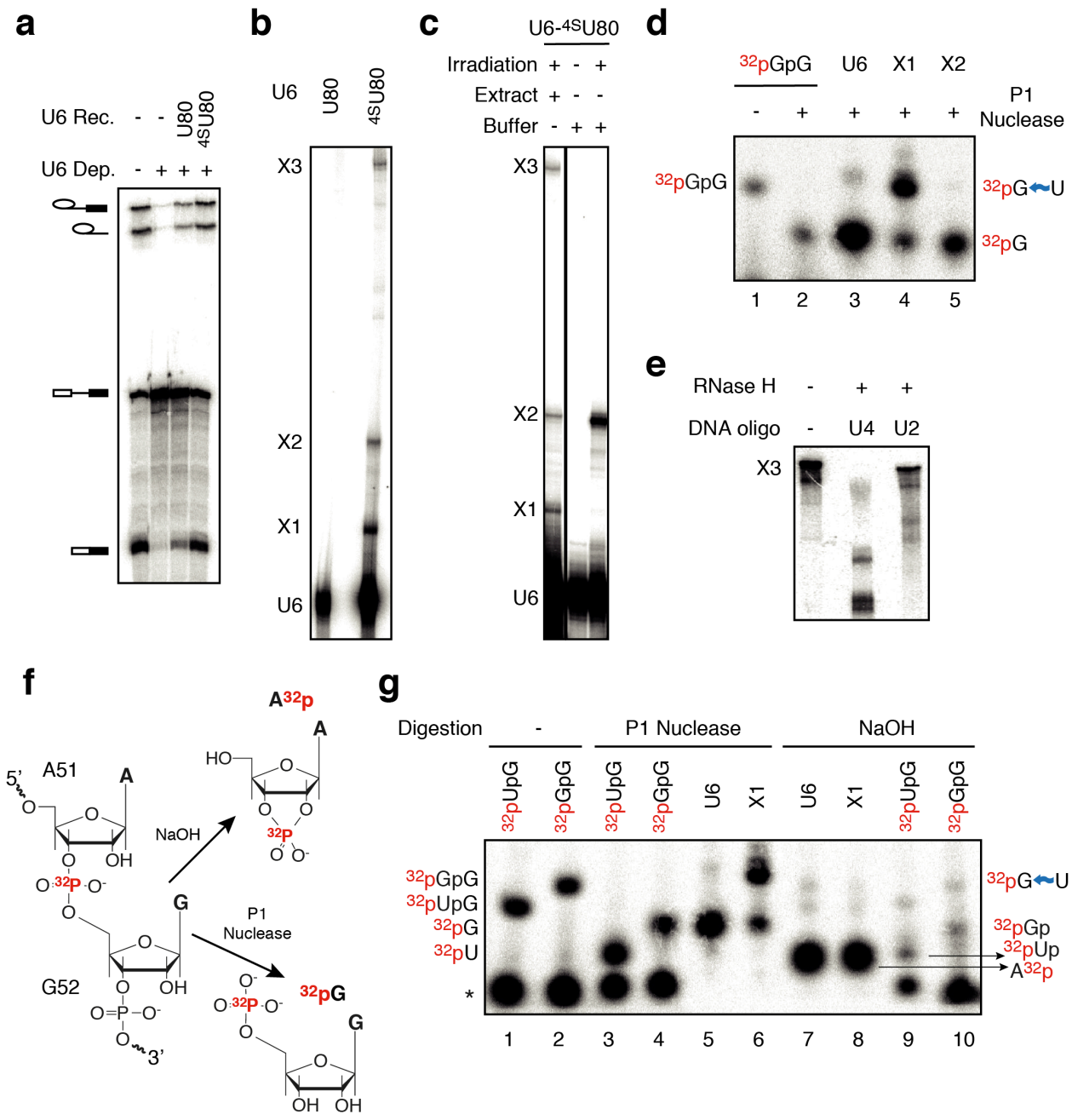

Supplementary Figure 2. Further characterization of U6-^{4S}U80 crosslinks. a, Denaturing PAGE analysis of *ACT1* pre-mRNA splicing by extracts reconstituted with the indicated synthetic U6 snRNA. Dep., depletion; Rec., reconstitution. **b-c,** Denaturing PAGE analysis of U6-^{4S}U80 recovered from *in vitro* splicing reactions after UV irradiation. Reactions were performed in the presence of unlabeled *ACT1* pre-mRNA. Note that X2 occurs more efficiently in buffer alone, whereas X1 and X3 require splicing extract. **d,** Denaturing PAGE analysis of RNA products following P1 nuclease digestion

of gel-purified U6, X1, and X2. Note that X2 digests to mononucleotides and thus does not involve an interaction between U80 and G52. **e,** Denaturing PAGE analysis of RNaseH digestion of gel-purified X1. Where indicated, DNA oligonucleotides complementary to U2 or U4 snRNA were used. Note that only the oligonucleotide complementary to U4 can direct RNaseH cleavage of X3, demonstrating that X3 involves an interaction between U80 and nucleotides in the U4 snRNA. **f-g,** Denaturing PAGE analysis of RNA products following analytic digestion of gel-purified U6, X1, and X2. Purified RNAs were digested as indicated (**g**). A diagram of the expected products in each case is also shown (**f**). The positions of the inferred products from the analytical digestions are indicated on the sides of the gel; * indicates unincorporated ^{32}pppA used for 5' end labeling. Note that, A^{32}p migrates similarly in lanes 7 and 8 to how ^{32}pUp migrates in lane 9.

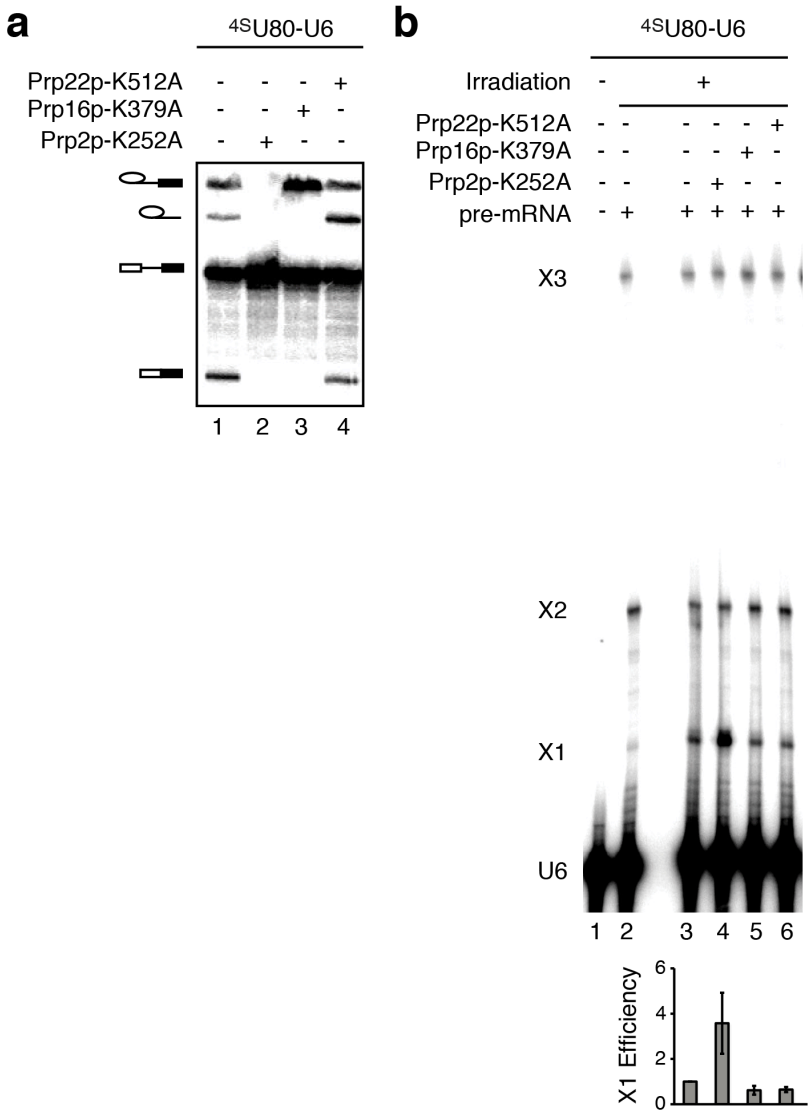

Supplementary Figure 3. The X1 crosslink can be detected in the presence of several dominant negative ATPases. a, Denaturing PAGE analysis of *ACT1* pre-mRNA splicing in the presence of the indicated recombinant proteins. Split reactions were set up with extracts used in **b** in the presence of radiolabeled *ACT1* pre-mRNA. **b,** Denaturing PAGE analysis of U6-^{4S}U80 recovered from *in vitro* splicing reactions after UV irradiation. Splicing was performed in the presence of unlabeled *ACT1* pre-mRNA. Error bars represent s.d. of three independent experiments.

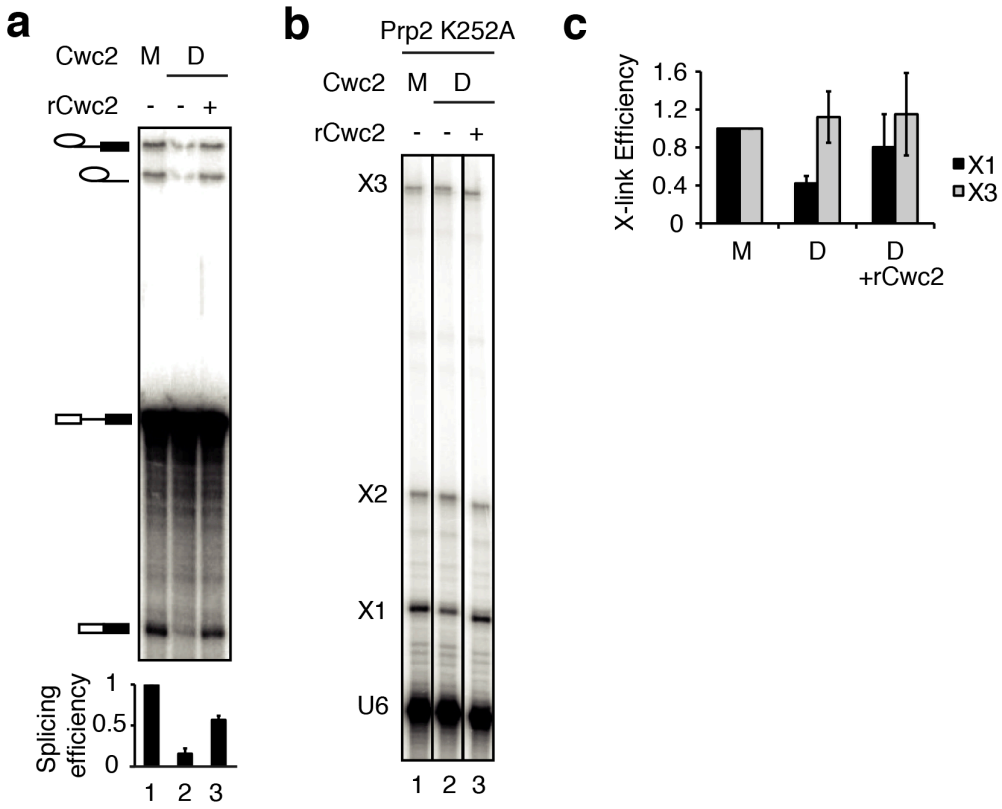

Supplementary Figure 4. Cwc2 promotes formation of the stacking interaction between U6-U80 and U6-G52. a, Denaturing PAGE analysis of splicing of ACT1 pre-mRNA in mock-depleted (M) and Cwc2p-depleted extracts (D) and reconstituted with U6-^{4S}U80. **b,** Denaturing PAGE analysis of U6-^{4S}U80 recovered from *in vitro* splicing reactions after UV irradiation. Splicing was performed in the presence of unlabeled *ACT1* pre-mRNA and Prp2p K252A was added in order to stall spliceosomes prior to the final stage of spliceosome activation and to increase the signal for the X1 crosslink. **c,** Quantification of crosslinking efficiency. Values were normalized to the efficiency observed for the mock-depleted extract. In **a** and **c** error bars denote s.d. of three technical replicates. Note that depletion of Cwc2p reduced by 2.5-fold the efficiency of X1 and addition of rCwc2 restored crosslinking efficiency to a level similar to that observed for the mock-depleted extract and in proportion to the levels Cwc2p restored splicing in the depleted extract (compare with **a**).

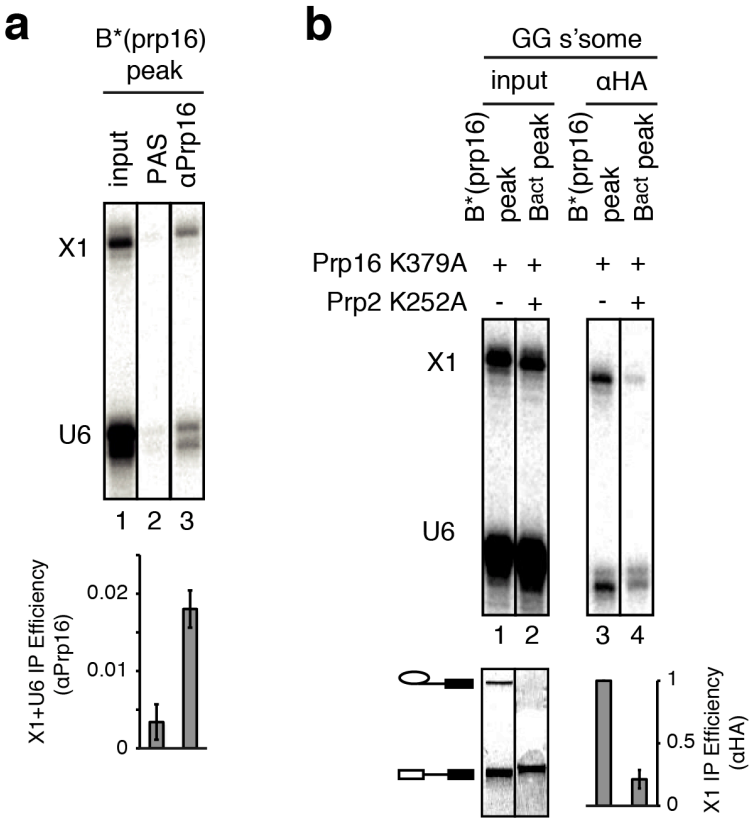

Supplementary Figure 5. The U6 triplex is present during branching and exon ligation: controls for the specific association of the X1 crosslink with Prp16p. a, Denaturing PAGE analysis of U6-^{4S}U80 recovered after UV irradiation and immunoprecipitation with Prp16p of the indicated complex isolated from glycerol gradient fractions illustrated in **Fig. 6b**. PAS, protein A-sepharose. Lower panel shows quantification of IP efficiency. Note that the anti-Prp16 antibody immunoprecipitated U6 and X1 5-fold above background binding to beads. **b,** Denaturing PAGE analysis of U6-^{4S}U80 recovered after UV irradiation and immunoprecipitation with Cwc25-HA of the indicated complexes isolated from glycerol gradient fractions illustrated in **Fig. 6b**. A representative gel for the input and immunoprecipitated material (αHA) from glycerol gradient-fractionated spliceosomes (GG s'some) is shown. The lower panel shows the *UBC4* substrate present in the fractions used for immunoprecipitation, detected by Cy3 channel, as well as quantification of X1 immunoprecipitation efficiency relative to the input. The X1 immunoprecipitation efficiency for the B^{act} peak (lane 4) was further normalized to that for the B$^{*(Prp16)}$ peak (lane 3), which was set to 1. Note that X1 is

enriched in the Cwc25p immunoprecipitate when spliceosomes have undergone Prp2-dependent activation (lane 3), and X1 is de-enriched in the immunoprecipitate from splicesomes stalled before the Prp2 step (lane 4). Error bars represent s.d. of three technical replicates.

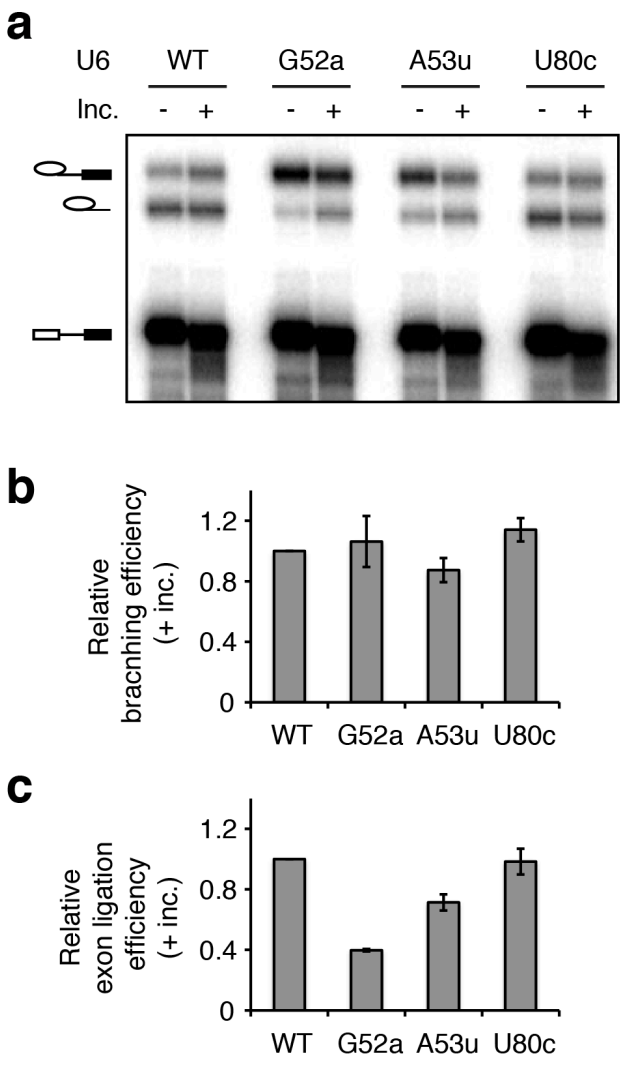

Supplementary Figure 6. U6 triplex mutations do not affect branching of the 3′O-PO substrate. a, Denaturing PAGE analysis of splicing of *UBC4* pre-mRNA by affinity-purified spliceosomes reconstituted with the indicated U6 variants. No dep., no depletion; no rec., no U6 reconstitution. (**b-c**) Quantification of branching (**b**) and exon ligation (**c**) efficiencies, normalized to wild-type. Spliceosomes from extracts reconstituted with the indicated U6 variants were assembled on the *UBC4* 3′O-PO substrate, affinity-purified via Prp19p and incubated in buffer PK (pH 7.0) with 1 mM $MgCl_2$. Splicing efficiencies were calculated for spliceosomes following affinity purification and subsequent incubation. Error bars represent s.d. of three technical replicates; inc., incubation.

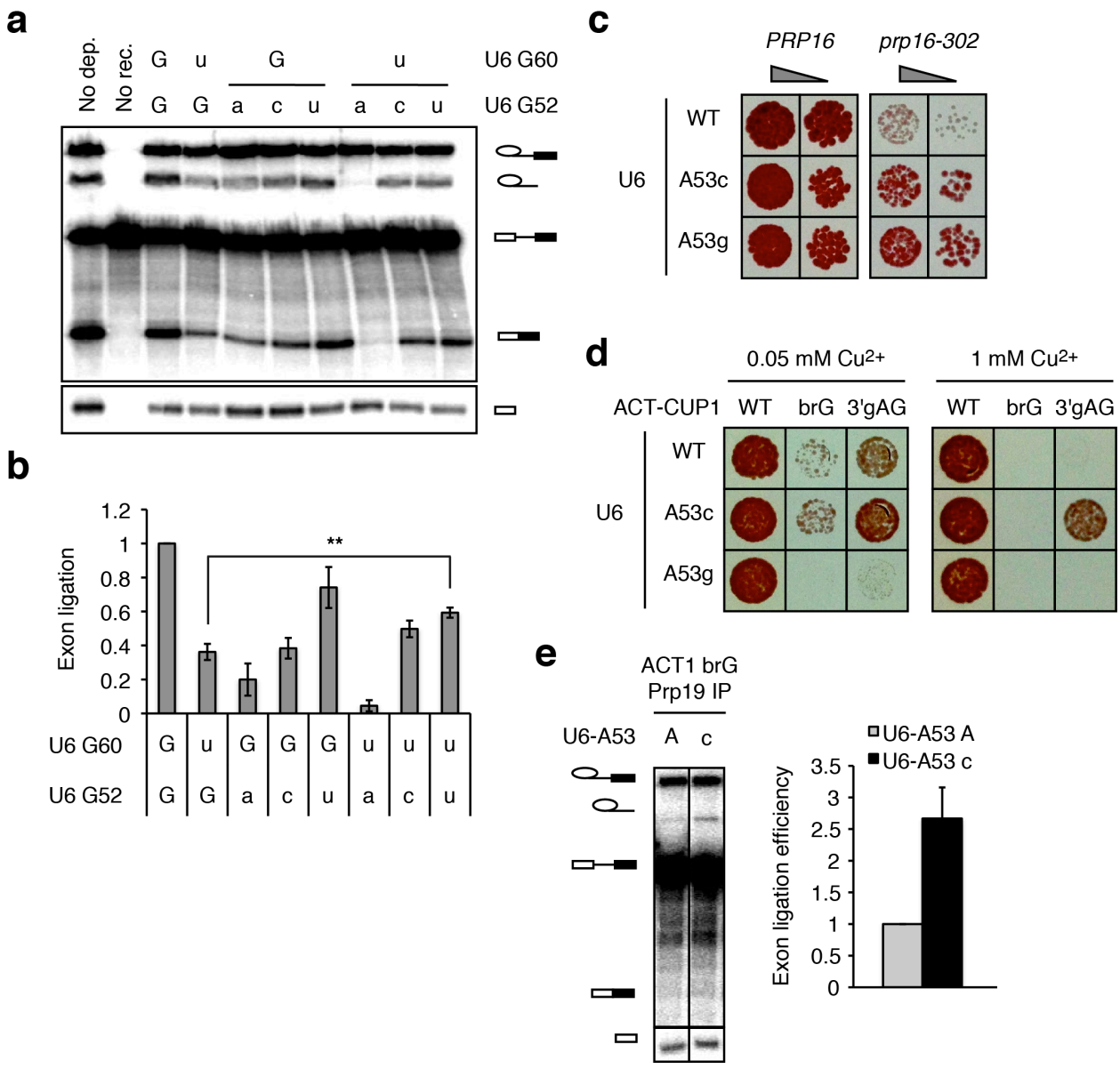

Supplementary Figure 7. Further evidence that the U6 triplex functions during both steps of splicing. **a,** Denaturing PAGE analysis of splicing of *ACT1* pre-mRNA in extracts reconstituted with the indicated U6 variants. No dep., no depletion; no rec., no U6 reconstitution. **b,** Quantififcation of exon ligation for the indicated U6 variants, normalized to wild-type U6; exon ligation was calculated as mRNA/lariat intermediate (ref. 2). The efficiency of branching was within 10% of wild-type for all U6 variants (quantification not shown). Error bars represent s.d. of four independent experiments; **, denotes statistical significance of the difference between the exon ligation efficiencies of

U6-G60U and U6-G60U/U6-G52U (p=0.0004, paired, 1-tailed, t-test). **c,** Spot assays showing growth on selective media of equivalent numbers of yeast cells expressing wild-type *PRP16* or *prp16-302* and containing the indicated U6 variants. Two 6-fold serial dilutions are shown. **d,** Spot assays showing ACT-CUP1 reporter-dependent growth of yeast containing the indicated U6 and ACT-CUP1 variants on media containing various concentrations of Cu^{2+}. **e,** Denaturing PAGE analysis of splicing of ACT1 brG pre-mRNA by extracts reconstituted with the indicated U6 variants. Spliceosomes from extracts reconstituted with the indicated U6 variants were assembled on an *ACT1* pre-mRNA bearing a guanosine at the branch site. To increase signal for the excised intron, spliceosomes were affinity-purified via Prp19p. The exon ligation efficiency was quantified without further incubation and is shown in the right panel as EI/(EI+LI), where EI is the excised intron and LI the lariat intermediate. Error bars represent s.d. of three technical replicates.

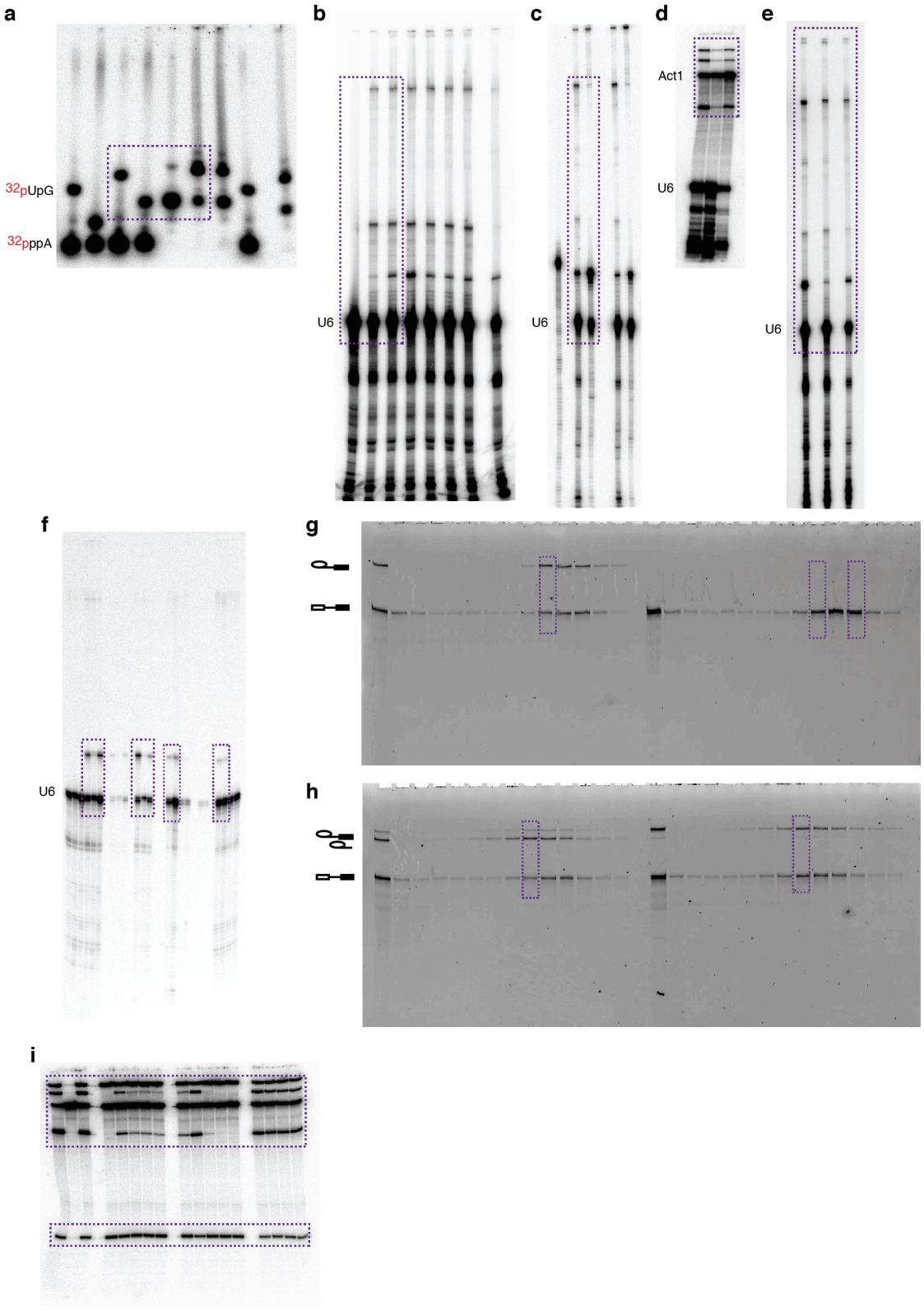

Supplementary Figure 8. Original images used to prepapre display items for the main figures. a, Full gel used for Fig. 4d. **b,** Full gel used for Fig. 4b. **c,** Full gel used for

Fig. 5a. **d,** Full gel used for Fig. 5b. **e,** Full gel used for Fig. 5c. **f,** Full gel used for upper panels in Fig. 6c and 6d. Note that the image shown in Fig. 6d is flipped along the vertical axis, relative to the full gel shown here. **g,** Full gel used for lower panel in Fig. 6c. **h,** Full gel used for lower panel in Fig. 6d. **i,** Full gel used for Fig. 8b.

SUPPLEMENTARY TABLES

Supplementary Table 1. Summary of synthetic lethal genetic interactions observed for combinations of mutations in the U6 triple helix

Non-paired combinations			Paired combinations		
Combination	**Number synthetic lethal of total[a]**	**%**	**Combination**	**Number synthetic lethal of total[a]**	**%**
A53•C61-G21	34 of 44	77%	U80•C61-G21	12 of 28	42%
G52•C61-G21	14 of 14	100%	G52•G60-C22	1 of 4	25%
A53•G60-C22	7 of 12	58%	A53•A59-U23	11 of 18	61%
U80•G60-C22	3 of 8	38%			
G52•A59-U23	6 of 6	100%			
U80•A59-U23	2 of 5	40%			
A53•U80	0 of 6	0%			
G52•U80	1 of 2	50%			

[a]The total combinations of mutations reported here for non-paired interactions (not in the same triple) and paired interactions (in the same triple) reflect only combinations in which the component mutations were viable (either on their own or in the context of repaired U2/U6 helix Ib). A synthetic lethal or synthetic enhancement interaction was defined as one in which the combination grew worse than the sickest of the component mutations. Note that for mutations that altered a helix Ib base pair and an out-of-plane base triple partner, the mutation combinations resulted in synthetic phenotypes in 75% of the cases.

Supplementary Table 2. Observed and predicted C1′-C1′ distances for base-triple partners

C1'-C1' distances (Å)				
Base triple	**U80•C61-G21**	**Group II intron**	C377•C360-G383	7.9[a]
		Spliceosome wild-type	U80•C61-G21	7.9[b]
		Spliceosome suppressor	C80•G61-C21	8.8[c]
	G52•G60-C22	**Group II intron**	G288•G359-U384	11.1[a]
		Spliceosome wild-type	G52•G60-C22	11.6[c]
		Spliceosome suppressor	U52•U60-A22	11.2[c]
	A53•A59-U23	**Group II intron**	C289•C358-G385	9.7[a]
		Spliceosome wild-type	A53•A59-U23	12.5[c]
		Spliceosome suppressor	C53•G59-C23	11.1[c]

a – observed in the group II intron structure (PDB 4FAQ)

b – predicted based on the group II intron structure (PDB 4FAQ)

c – predicted based on modeling or similar interactions observed crystallographcally[S6]

SUPPLEMENTARY NOTES

Supplementary Note 1. The exhaustive extent of our genetic tests for base-triple interactions in U6

Our mutational analysis was exhaustive. We tested all possible allele combinations for each of the three predicted U6 base-triple interactions – alone and in combination with mutations at the third (U2) position of each triple and/or with repair of the U4/U6 duplex. Thus, we tested 384 mutants for suppression. While we tested all possible allele combinations, we were particularly interested in genetic interactions revealing suppression of phenotypic AGC triad mutations. In addition, to test for positional specificity of suppression within the triple helix, we combined each third strand allele with all possible alleles combinations at the each of the two helix Ib base pairs of the predicted, flanking base-triples, and we tested two thirds of all possible combinations of third-strand mutations. Thus, we performed 416 positional specificity tests. In all, we tested 800 mutants, nearly saturating mutagenesis of the predicted base-triple interactions. For simplicity, we present only the suppressors we identified alongside select specificity controls at each position; we summarize remaining interactions in **Supplementary Table 1**.

Supplementary Note 2. Tolerance of various bases at critical positions of the predicted U6 triplex

We note that the triplex in group IIA/B introns, predicted from the analogous triplex observed crystallographically in the group IIC intron[S1], differs from the triplex in

the spliceosome at only two of the nine bases, and substitution of either base in the spliceosome with the corresponding base from the group II intron supports growth (**Fig. 2**, refs. S2,S3). Moreover, the tolerance of specific mutations at critical positions in the U6 base-triples parallels that observed for the group II intron. Specifically, the tolerance of the U80A mutation in U6 (**Fig. 2a**) parallels the occasional presence of an adenosine at the equivalent, bulged position in domain V of group II introns, where an adenosine has been proposed to interact with the AGC triad in a manner analogous to a cytosine[S1]. Similarly, the ability of both A and U to substitute for G60 in the spliceosome (**Fig. 3a**, ref. S2) parallels a similarly ability of A and U to substitute for the analogous residue in the group II intron[S4].

Supplementary Note 3. Suppression of U6-G60U required relative stabilization of U4/U6 stem I.

Suppression of U6-G60U by U6-G52U (**Fig. 3a**) required a mutation in U4 snRNA at U4-C59, which could repair base-pairing with U6-G60U in U4/U6 stem I, although base-pairing was not required since any mutation at the corresponding U4 position permitted suppression (M.A.M. and J.P.S. unpublished, compare with ref. S2). These data suggest that U4-C59 may form an interaction that competes with a structure involving U6-G60 such that mutation of U4-C59 disrupts the competing structure and restores an equilibrium between the two structures. Indeed, U4-C59 mutations would disrupt the intramolecular U4 stem I (ref. S5) and could thereby re-favor formation of the mutually exclusive U4/U6 stem I, disrupted by U6-G60U.

Supplementary Note 4. Position and allele specificity of suppression observed for mutations at G60 and A59.

Suppression of G60U was allele- and position-specific. For example, G52U failed to suppress other mutations at G60 (**Fig. 3a**) and failed to suppress mutations at the other two positions in the AGC triad, such as C61G, and A59U (**Fig. 3b**, **Supplementary Fig. 1b**), which were, by contrast, suppressed by mutations in their respective, predicted base-triple partners (**Fig. 2a**; see below); indeed, G52U exacerbated mutations at C61 and A59 (**Fig. 3b**, **Supplementary Table 1**).

Mutations at A59 showed a more complex suppression pattern. Although A53C suppressed all three alleles at position A59, suppression was position-specific, because A53 mutations did not suppress mutations at the other AGC triad positions, such as U6-C61 or U6-G60 (**Fig. 3d**, **Supplementary Fig. 1d**), which were, by contrast, suppressed by their respective, predicted base-triple partners (**Figs. 2a, 3a**); indeed, A53 mutations exacerbated mutations at C61 and G60 (**Fig. 3d**, **Supplementary Table 1**). Additionally, in the case of A59U, repair of U2/U6 helix Ib allowed any mutation of A53 to suppress (**Fig. 3c**); the breadth of these suppressors may indicate that they disrupt an aberrant Watson-Crick base pair that could form between A53 and the A59U mutation, which could contribute to the lethality of this mutation.

Supplementary Note 5. Predicted isomorphic interactions for base-triple suppressors

At the U6-U80•U6-C61/U2-G21 base triple, when U6-U80C suppresses U6-C61G/U2-G21C, besides the predicted interaction between O6 of C61G and N4 of U80C, protonation of N3 of cytosine, as has been suggested based on crystallographic data[S6] and observed directly by NMR (ref. S7), would allow a hydrogen bond between N3 of U80C and N7 of C61G (not shown). Additionally, the group II structure suggests an alternative to the predicted interaction between O6 of C61G with N4 of U80C. Specifically, N4 of U80C could interact with O4′ of the G52 ribose sugar. This would likely give C1′-C1′ distances that are the same as those observed in the group II structure. Notably, such an interaction with the O4′ of G52 would be maintained in the case of the U80A mutation by N6 of adenosine. Furthermore, the N3 position of adenosine could interact with the N4 position of cytosine just as the O2 position of uracil and cytosine cans[S1]. These latter two alternative interactions would explain the viability of U80A in the context of a triplex.

At the U6-G52•U6-G60/U2-C22 base triple, we expect N1 and N2 of U6-G52 to interact with N7 and O6 of U6-G60, respectively, just as G288 interacts with G359 in the group II intron (**Figs. 1c, 3e**). When U6-G52U suppresses the defect of U6-G60U U2-C22, the N3 of U6-G52U can interact with O4 of U6-G60U (**Fig. 3e**).

At the final position of the group II intron triplex, a non-canonical base triple forms in which N4 of C289 not only interacts with C358 through the base, via an interaction between O2 of C289 and N4 of C358, but also through the backbone, via a hydrogen

bond with the *pro-R*$_P$ non-bridging oxygen (**Fig. 1c**; refs. S1,S8). In the spliceosome, this base triple is replaced by U6-A53•U6-A59/U2-U23, in which A53 could interact with A59 through the base, via interactions between N1 and N6 of A53 and N6 and N7 of A59, respectively (**Fig. 3f**), as was recently proposed for the spliceosome as well as the IIA/IIB class of group II introns[S1]. Interestingly, U6-A53C could potentially also interact with A59 through the backbone, in analogy to C289 of the group II triplex, via an interaction between N1 of A53 the *pro-R*$_P$ non-bridging oxygen of U6-A59. This interaction would not be expected to form in the wild-type A53 context (see ref. S1 for modeling of the A-A geometry at the analogous position in group II). However, in the context of a disrupted helix Ib, the interaction with the phosphate backbone may allow A53C to keep the phosphate backbone of A59 in the proper position for catalytic metal binding by A59 and at the same time recruit the ACAGAGA sequence to the catalytic core. This possibility could explain why the integrity and identity of helix Ib is not as critical in the A53C background.

Supplementary Note 6. Alternative mechanism of suppression at A59

A53C may suppress mutations broadly at A59 by destabilizing a competing structure. In this view, A53C only suppresses mutations at A59 and not other positions of the triad because the A59 mutations have already disrupted an interaction between A53 and A59, so the A53C mutation cannot further destabilize the triple. Consequently, only in the context of A59 mutations, A53C specifically destabilizes the competing conformation, thereby suppressing A59 mutations in a positionally-specific manner. This

indirect mechanism of suppression would rationalize the breadth of mutations suppressed at the A59-U23 helix Ib base pair. We cannot therefore exclude the possibility that the precise structure of the A53-A59 interaction is less important than its relative stability, which could also be buffered by proteins that scaffold the active site[S9-S11].

Supplementary Note 7. The X1 crosslink does not involve linkage between U80 and A51

Since the equivalent of A51 is also in close proximity to the equivalent of U80 in the group II intron structure[12], we sought to rule out that U80 was crosslinking to A51. We therefore subjected X1 to alkaline hydrolysis, which degrades RNA to single nucleotide 3′-cyclic monophosphates (**Supplementary Fig. 2f**). In this case the radioactive label should be transferred to A51, as a 3′-cyclic phosphate, and a shift, relative to mononucleotide, should be observed for X1 if A51 were involved in the interaction. However, both uncrosslinked U6-^{4S}U80 and X1 digested to species migrating as mononucleotides (**Supplementary Fig. 2g**), eliminating the possibility that the crosslink could represent an interaction between U80 and A51 and confirming that X1 reports on a direct stacking interaction between U80 and G52.

Supplementary Note 8. Justification for the use of 4-thio-uridine crosslinking as a tool to detect stacking interactions between residues involved in the U6 triple helix

A crosslink between two residues could formally indicate interactions in a variety of conformations. Nonetheless, the chemistry of 4-thio-uridine photocrosslinking requires some degree of stacking[S13], given that this crosslinking reaction proceeds through a thietane intermediate that results from interactions between two pairs of stacked, π orbitals. Thus, efficiently crosslinked residues have been shown to stack. Indeed, in the first documented case of 4-thio-uridine crosslinking, in tRNA-Val (ref. S14), the crosslinked residues, which crosslinked with more than 50% efficiency, were later shown to stack (PDB 2K4C; ref. S15). We similarly observed greater than 50% crosslinking efficiency in activated spliceosomes (**Fig. 5a**), strongly implying a stable interaction between these residues. Moreover, in the group II intron, a 4-thio-uridine crosslink has been observed between the residues equivalent to U80 and G52 (ref. S16), the two residues we have crosslinked in the spliceosome. Thus, in the context of our previous study revealing that U6 and the catalytic domain of the group II intron utilize five stereochemically equivalent ligands to bind two catalytic metals and given that a triplex organizes these ligands in the group II intron, the simplest interpretation of our crosslink between U80 and G52 is that these residues stack as a result of participating in a triple helix interaction.

Supplementary Note 9. Cwc2 promotes the U6 triplex.

Consistent with a role for the NTC in stabilizing the U6 triplex, we found that Cwc2p, which associates with the NTC (ref. S17), promotes formation of the X1 crosslink (**Supplementary Fig. 4**). Interestingly, Cwc2p also protects the two catalytically important triplex components – the U80 bulge and helix Ib – from chemical modification in B^{act} complexes[S10]. Thus, our results support the previous proposition that Cwc2p stabilizes formation of catalytic structures in U6, substituting for RNA structures that in the group II intron stabilize the catalytic configuration of domain V (ref. S10).

Supplementary Note 10. Additional controls supporting the formation of X1 in spliceosomes stalled at the branching stage.

As an additional control for formation of X1 specifically in the B*(prp16) complex (**Fig. 6c**), we blocked formation of the B*(prp16) complex by adding rPrp2p-K252A to splicing reactions, which would also shift spliceosomes deeper into the gradient (**Fig. 6b**). Then, we isolated any residual complexes from the region of the glycerol gradient where the B*(prp16) complex would have migrated. In contrast to genuine B*(prp16) complex spliceosomes, the residual co-migrating complexes, reflected by uncrosslinked U6, did not support efficient X1 formation (**Fig. 6c**, lane 2, top). These results indicate that that the crosslink observed in this region of the gradient required Prp2p, consistent with the crosslink forming in B*(prp16) complex spliceosomes stalled just after branching.

In further support of this idea, Cwc25p specifically immunoprecipitated X1 from

fractions of the B*(prp16) complex peak (**Supplementary Fig. 5b**).

Supplementary Note 11. Mutations in the predicted base-triple partners do not compromise branching for a substrate that is not limiting for catalytic metal ion binding

In contrast to their deleterious effect on rescue of the 3′S-PS(R_P) substrate, specific mutations predicted to disrupt the U6 base-triple partners (U6-G52A and U6-A53U) did not significantly compromise branching for a wild-type substrate (3′O-PO; **Supplementary Fig. 6**). This suggests that G52A and A53U are normally not limiting for branching of the 3'O-PO substrate. The fact that branching becomes sensitive to G52A and A53U only when catalytic metal ion binding at the 5′ splice site is perturbed provides further evidence that the triplex specifically functions during branching.

Supplementary Note 12. Possible role of the triplex in recruiting the 3′ splice site.

The triplex could help to recruit the 3′ splice site to the catalytic core either through the proposed non-Watson-Crick interaction between the last nucleotide of the intron and the first nucleotide of the intron[S18], which itself would be positioned by the ACAGAGA sequence, or through an interaction between U6-A51, immediately adjacent to the triplex, and the 3′ splice site. This latter interaction would be analogous to the interaction responsible for 3′ splice site recruitment to the catalytic core of the group II intron, in which the J2/3 linker, through a residue equivalent to U6-A51, pairs to the last residue of the intron at the 3′ splice site forming the γ-γ' interaction[S19]. In this context, it

is noteworthy that mutations at U6-A51 severely and specifically compromise exon ligation *in vitro*[S20].

SUPPLEMENTARY REFERENCES

S1. Keating, K. S., Toor, N., Perlman, P. S. & Pyle, A. M. A structural analysis of the group II intron active site and implications for the spliceosome. *RNA* **16,** 1–9 (2010).

S2. Hilliker, A. K. & Staley, J. P. Multiple functions for the invariant AGC triad of U6 snRNA. *RNA* **10,** 921–928 (2004).

S3. McManus, C. J., Schwartz, M. L., Butcher, S. E. & Brow, D. A. A dynamic bulge in the U6 RNA internal stem-loop functions in spliceosome assembly and activation. *RNA* **13,** 2252–2265 (2007).

S4. Konforti, B. B. *et al.* Ribozyme catalysis from the major groove of group II intron domain 5. *Mol Cell* **1,** 433–441 (1998).

S5. Myslinski, E. & Branlant, C. A phylogenetic study of U4 snRNA reveals the existence of an evolutionarily conserved secondary structure corresponding to 'free' U4 snRNA. *Biochimie* **73,** 17–28 (1991).

S6. Leontis, N. B., Stombaugh, J. & Westhof, E. The non-Watson-Crick base pairs and their associated isostericity matrices. *Nucleic Acids Res* **30,** 3497–3531 (2002).

S7. Cash, D. D. *et al.* Pyrimidine motif triple helix in the Kluyveromyces lactis telomerase RNA pseudoknot is essential for function in vivo. *Proc. Nat. Acad. Sci. USA* **110,** 10970-10975 (2013).

S8. Toor, N., Keating, K. S., Taylor, S. D. & Pyle, A. M. Crystal structure of a self-spliced group II intron. *Science* **320,** 77–82 (2008).

S9. Galej, W. P., Oubridge, C., Newman, A. J. & Nagai, K. Crystal structure of Prp8 reveals active site cavity of the spliceosome. *Nature* **493,** 638–643 (2013).

S10. Rasche, N. *et al.* Cwc2 and its human homologue RBM22 promote an active conformation of the spliceosome catalytic centre. *EMBO J* **31,** 1591–1604 (2012).

S11. Anokhina, M. *et al.* RNA structure analysis of human spliceosomes reveals a compact 3D arrangement of snRNAs at the catalytic core. *EMBO J* **32**, 2804-2818 (2013).

S12. Chan, R. T., Robart, A. R., Rajashankar, K. R., Pyle, A. M. & Toor, N. Crystal structure of a group II intron in the pre-catalytic state. *Nat Struct Mol Biol* **19**, 555-557 (2012).

S13. Favre, A., Saintomé, C., Fourrey, J. L., Clivio, P. & Laugâa, P. Thionucleobases as intrinsic photoaffinity probes of nucleic acid structure and nucleic acid-protein interactions. *J. Photochem. Photobiol. B, Biol.* **42,** 109–124 (1998).

S14. Yaniv, M., Favre, A. & Barrell, B. G. Structure of transfer RNA: evidence for interaction between two non-adjacent nucleotide residues in tRNAVal1 from Escherichia coli. *Nature* **223,** 1331–1333 (1969).

S15. Grishaev, A., Ying, J., Canny, M. D., Pardi, A. & Bax, A. Solution structure of tRNAVal from refinement of homology model against residual dipolar coupling and SAXS data. *J. Biomol. NMR* **42,** 99–109 (2008).

S16. de Lencastre, A. & Pyle, A. M. Three essential and conserved regions of the group II intron are proximal to the 5'-splice site. *RNA* **14,** 11–24 (2008).

S17. Ohi, M. D. & Gould, K. L. Characterization of interactions among the Cef1p-Prp19p-associated splicing complex. *RNA* **8,** 798–815 (2002).
S18. Parker, R. & Siliciano, P. G. Evidence for an essential non-Watson-Crick interaction between the first and last nucleotides of a nuclear pre-mRNA intron. *Nature* **361,** 660–662 (1993).
S19. Jacquier, A. & Michel, F. Base-pairing interactions involving the 5′ and 3′-terminal nucleotides of group II self-splicing introns. *J Mol Biol* **213,** 437–447 (1990).
S20. Fabrizio, P. P. & Abelson, J. J. Two domains of yeast U6 small nuclear RNA required for both steps of nuclear precursor messenger RNA splicing. *Science* **250,** 404–409 (1990).